Delithiation/Lithiation Behavior of $LiNi_{0.5}Mn_{1.5}O_4$ Studied by *In Situ* and *Ex Situ* ^{6,7}Li NMR Spectroscopy

Keiji Shimoda,*[,†] Miwa Murakami,[†] Hideyuki Komatsu,[†] Hajime Arai,[†] Yoshiharu Uchimoto,[‡] Zempachi Ogumi[†]

[†]Office of Society-Academia Collaboration for Innovation, Kyoto University, Uji, Kyoto 611-0011, Japan

[‡]Graduate School of Human and Environment Studies, Kyoto University, Kyoto 606-8501, Japan

Abstract

Delithiation and lithiation behaviors of ordered spinel $LiNi_{0.5}Mn_{1.5}O_4$ and disordered spinel $LiNi_{0.4}Mn_{1.6}O_4$ were investigated by using *in situ* (*in operando*) ^{7}Li NMR and *ex situ* ^{6}Li MAS NMR spectroscopy. The *in situ* ^{7}Li monitoring of the ordered spinel revealed a clear appearance and subsequent disappearance of a new signal from the well-defined phase $Li_{0.5}Ni_{0.5}Mn_{1.5}O_4$, suggesting the two-phase reaction processes among $Li_{1.0}Ni_{0.5}Mn_{1.5}O_4$, $Li_{0.5}Ni_{0.5}Mn_{1.5}O_4$, and $Li_{0.0}Ni_{0.5}Mn_{1.5}O_4$. Also, for the disordered spinel, $Li_{0.5}Ni_{0.4}Mn_{1.6}O_4$ was identified with a broad distribution in Li environment. High-resolution ^{6}Li MAS NMR spectra were also acquired for the delithiated and lithiated samples to understand the detailed local structure around Li ions. We suggested that the nominal Li-free phase $Li_{0.0}Ni_{0.5}Mn_{1.5}O_4$ can accommodate a small amount of Li ions in its structure. The

tetragonal phases $Li_{2.0}Ni_{0.5}Mn_{1.5}O_4$ and $Li_{2.0}Ni_{0.4}Mn_{1.6}O_4$, which occurred when the cell was discharged down to 2.0 V, were very different in Li environment from each other. It is found that ^{6,7}Li NMR is highly sensitive not only to the Ni/Mn ordering in $LiNi_{0.5}Mn_{1.5}O_4$ but also to the valence changes of Ni and Mn on charge-discharge process.

Keywords: Nuclear magnetic resonance, *in situ* NMR, lithium ion rechargeable battery, $LiNi_{0.5}Mn_{1.5}O_4$.

Corresponding author:

Keiji Shimoda

Gokashou, Uji 611-0011, Japan

Center for Advanced Science and Innovation, Kyoto University

E-mail address: k-shimoda@saci.kyoto-u.ac.jp

Tel: +81-774-38-4967

Fax: +81-774-38-4996

1. Introduction

Lithium ion rechargeable batteries (LIBs) have been widely used as a power source for portable devices and now are available for applications to electric vehicles (EVs), which demand high-power, high-energy, inexpensive and safe batteries.[1–3] A nickel-substituted lithium manganese spinel $LiNi_{0.5}Mn_{1.5}O_4$ has been extensively studied as a preferred candidate of high-voltage positive electrode materials because it shows a wide potential plateau at ~4.7 V vs. Li/Li^+ as well as its low toxic nature.[4,5] This material shows two distinct cubic structures depending on the Ni and Mn distribution.[6–11] In the Ni/Mn ordered structure, Ni^{2+} and Mn^{4+} ions occupy the 4*b* and 12*d* Wyckoff positions in the space group $P4_332$, respectively, while these ions randomly occupy the 16*d* position in the Ni/Mn disordered *Fd*-3*m* structure. It is believed that the cation ordering is an important factor influencing battery performances, and several studies reported better cycling performance and rate capability for the disordered spinel,[6,7,9] whereas a recent study has suggested that the partially ordered spinel having integrated nano-domains of ordered and disordered structures shows better performances than each spinel does.[12] The disordered spinel is often prepared by the calcination at higher temperatures, which provides oxygen loss and is sometimes expressed as $LiNi_{0.5}Mn_{1.5}O_{4-\delta}$.[6,8,13] Alternatively, Cabana *et al.* suggested that the disordered spinel prepared at high temperatures systematically showed an excess of Mn, which was compensated by the formation of a secondary rock-salt phase but not by the creation of oxygen vacancies, *i.e.*, $LiNi_{0.5-\delta}Mn_{1.5+\delta}O_4$.[10,14]

A small difference in delithiation process has been reported between the two spinel structures.[6,7,9] The delithiation of the $P4_332$ spinel basically proceeds in separate two-phase reactions between $LiNi_{0.5}Mn_{1.5}O_4$ ($Li_{1.0}$ phase) and $Li_{0.5}Ni_{0.5}Mn_{1.5}O_4$ ($Li_{0.5}$) at ~4.70 V, and

between $Li_{0.5}Ni_{0.5}Mn_{1.5}O_4$ and $Ni_{0.5}Mn_{1.5}O_4$ ($Li_{0.0}$) at ~4.74 V. On the other hand, the *Fd*-3*m* spinel shows a single-phase reaction (solid solution behavior) in the $Li_{1.0}$ phase at the initial stage of delithiation. Importantly, these phase transitions occur in a topotactic way, where the cubic lattice constant decreases from a = 8.17 Å ($Li_{1.0}$) to 8.09 Å ($Li_{0.5}$), and 8.00 Å ($Li_{0.0}$), respectively.[6,7,9,15] Such a small lattice mismatch (lattice strain) and a fast three-dimensional Li diffusion path would expect good rate capability and cyclability. X-ray absorption fine structure (XAFS) studies at Ni/Mn *K*- and $L_{2,3}$-edges have revealed that Ni^{2+} ions in the $Li_{1.0}$ phase was oxidized to Ni^{3+} in the $Li_{0.5}$ phase and Ni^{4+} in the $Li_{0.0}$ phase, respectively, while the valence state of Mn^{4+} ions remained unchanged during delithiation.[16–20]

Solid-state nuclear magnetic resonance (NMR) spectroscopy is a useful technique for investigating the chemical environments on a specific element in the battery materials. In particular, the ^{6,7}Li magic-angle spinning (MAS) NMR technique has been widely applied for the chemical structure characterization of the pristine and delithiated positive electrode materials, because it gives direct information about mobile Li^+ ions.[21–37] Cabana *et al.* compared the ^{6}Li MAS NMR spectra of $LiNi_{0.5}Mn_{1.5}O_4$ synthesized at various temperatures.[10] They suggested the existence of minor peaks other than that corresponding to a regular Li environment, and the relative intensities of the minor peaks are temperature-dependent. The sample with the $P4_332$ structure synthesized at 700 °C seems to show a relatively narrow distribution with a least amount of minor peaks, while that with the *Fd*-3*m* structure calcined at lower and higher temperatures shows a much broader distribution. ^{6}Li MAS NMR spectra for the $Li_xNi_{0.5}Mn_{1.5}O_4$ samples prepared at various states of charge were also reported, which showed that the signal intensity decreased

monotonously without any observable peak shifts or new resonances.[28] The authors concluded that the local electronic and atomic environments of the Li ions remaining in the structure were not significantly perturbed by the removal of the nearby Li ions. However, this is surprising, since the *in situ* X-ray diffraction (XRD) and XAFS results have clearly shown the structural and electronic evolutions on phase transition.[7,18] This apparent inconsistency may come from undesirable reaction in disassembling the batteries because it is expected that the active materials at charged state are highly reactive with moisture and oxygen. In recent years, *in situ* (*in operando*) static NMR measurements have been applied to small homemade batteries under electrochemical operation.[38–48] This technique enables us to quantitatively evaluate the spectral (structural) changes in a single experiment in a non-destructive manner, despite giving worse spectral resolution compared to the *ex situ* MAS technique. We here examine the delithiation and lithiation behavior of ordered spinel $LiNi_{0.5}Mn_{1.5}O_4$ and disordered spinel $LiNi_{0.4}Mn_{1.6}O_4$ by using *in situ* ^{7}Li NMR and *ex situ* ^{6}Li MAS NMR spectroscopy to clarify the correlation between crystal structures (Ni/Mn ordering) and Li local environments.

2. Experimental

The *P*4$_3$32-structured $LiNi_{0.5}Mn_{1.5}O_4$ was prepared by annealing the battery grade $LiNi_{0.5}Mn_{1.5}O_4$ powder ($Li_{1.002}Ni_{0.507}Mn_{1.496}O_{4.000}$, Toda Kogyo) at 700 °C for 48 h in air. Similarly, the *Fd*-3*m*-structured $LiNi_{0.4}Mn_{1.6}O_4$ was prepared by annealing the powder at 900 °C for 6 h. These structures were confirmed by X-ray diffraction and Raman spectroscopy. Energy-dispersive X-ray spectrometry (EDS) analyses on scanning electron microscope (SEM) showed the average Ni/Mn ratio of 0.48(1)/1.52(1) for the former

particles and 0.36(2)/1.64(2) for the latters (total of Ni and Mn amount was fixed to 2.0), indicating that annealing at high temperature causes the deviation of Ni/Mn ratio from the original one. A mixture of active material ($LiNi_{0.5}Mn_{1.5}O_4$ or $LiNi_{0.4}Mn_{1.6}O_4$), acetylene black (Denki kagaku Kogyo), polyvinylidene difluoride (PVDF, Kureha) with a weight ratio of 91 : 6 : 3 was spread with N-methylpyrrolidone (NMP) onto aluminum foil, and then dried at 80 °C under vacuum overnight to constitute a positive electrode. The SEM images of the electrodes were shown in Figure S1 (the average particle size; ~5 μm). The electrode for *in situ* NMR measurement was cut in the dimensions of 15 × 5 mm^2, which included ~15 mg of active material, while those for *ex situ* NMR, XRD, and Raman spectroscopic examinations were cut in the dimensions of 25 × 15 mm^2. A foil of metallic lithium (0.2 mm in thickness, >99.9 %, Honjo Metal) was used as a counter electrode. The electrolyte used in this study was 1 M $LiPF_6$ dissolved in anhydrous ethylene carbonate (EC) and ethylmethyl carbonate (EMC) with a volumetric ratio of 3 : 7 (Kishida Chemical). These components were assembled together with the Celgard 2500 separator and soaked in the electrolyte solution in an Ar-filled glove box (<3.0 ppm oxygen), which were sealed in a silica-coated or aluminum-coated plastic bag cells for *in situ* or *ex situ* NMR measurements, respectively.

The electrochemical measurements were performed at room temperature on an automatic cycling/data recording system (HJ1001SD8, Hokuto Denko). The cells were galvanostatically pre-cycled 3 times over the voltage range from 3.5 V to 5.0 V at a rate of 0.2C (1C = 147 mA/g), and then charged again to 5.0 V at a rate of 0.1C with a 5.0 V constant voltage charging process (10 h in total) and subsequently discharged to 2.0 V at a

rate of 0.1C with a 2.0 V constant voltage discharging process (20 h in total) for *in situ* NMR observation. A series of electrode samples for *ex situ* measurements were prepared in the same charge-discharge procedure and disassembled at desired states of charge and discharge. An electrode sample, which was soaked in the electrolyte solution for 48 h at room temperature but electrochemically uncycled, was also prepared for reference. They were carefully disassembled in the glove box, and rinsed with dimethyl carbonate (DMC) to remove the electrolyte solution residue. These samples were used for ^{6}Li MAS NMR, XRD, and Raman spectroscopic measurements.

In situ ^{7}Li NMR and ^{6}Li MAS NMR spectra were acquired on a DD2 600 spectrometer (Agilent Technologies) at a magnetic field of 14.1 T. *In situ* ^{7}Li NMR measurements were performed with a homemade wide-bore static probe, where a flat battery cell was vertically placed in the center of 10 mm diameter solenoidal coil.[44] A Hahn echo pulse sequence ($\pi/2$-τ-π-τ-acq.) was used with a first pulse width of 2.0 μs, echo decay of 8 μs and a relaxation delay of 0.05 s. We confirmed that the very short relaxation delay of 0.05 s was sufficient to obtain the full of intensity of spinel phases at several states of charge/discharge; the initial state (before charging), half-charged state, and discharged state at 2.0 V. The pulse irradiation offset frequency was set at the peak top position of $LiNi_{0.5}Mn_{1.5}O_4$ or $LiNi_{0.4}Mn_{1.6}O_4$ positive electrode material at the initial state during the *in situ* measurement. A total of 17916 scans was collected for each spectrum. It takes 15 min over which the acquired spectrum is averaged, corresponding to the change of 0.025Li per $LiNi_{0.5}Mn_{1.5}O_4$ in the 0.1C measurement. ^{6}Li MAS NMR measurements were performed with a wide-bore T3 MAS probe (Agilent Technologies). The powder samples were packed

into 1.2 mmϕ MAS ZrO_2 rotors with airtight caps, which were spun at a spinning rate of 40 or 60 kHz during the experiments. Although all the experiments were nominally carried out at room temperature, the practical temperatures of spinning samples at 40 and 60 kHz were estimated to be ~47 and ~67 °C, respectively, due to frictional heating, which were estimated based on a separate temperature calibration using ^{207}Pb NMR for $Pb(NO_3)_2$.[49] A rotor-synchronized Hahn echo sequence was used with a $\pi/2$ pulse width of 0.8 μs and a relaxation delay of 0.1 s. All spectra were referenced to 1M LiCl solution at 0.0 ppm.

3. Results and Discussion

3-1. *In situ* observation of Li structural changes in ordered and disordered spinel

Figure 1 shows the *in situ* ^{7}Li NMR spectra of Li//$LiNi_{0.5}Mn_{1.5}O_4$ cell along with an electrochemical profile charging from 3.5 V to 5.0 V and subsequent discharging down to 2.0 V (Figure 1a). The charge and discharge capacities were 132 and 241 mAh/g, respectively, indicating that $Li_{0.1}Ni_{0.5}Mn_{1.5}O_4$ and $Li_{1.74}Ni_{0.5}Mn_{1.5}O_4$ remained as bulk composition in the electrode neglecting any contributions from electrolyte decomposition and impurities in the active material. Three signals were observed in the lowermost spectrum before charging (Figure 1b). Sharp peaks at ~0 and 268 ppm are assigned to $LiPF_6$ in the electrolyte solution and Li metal as counter electrode, respectively. A severely broadened signal centered at ~1600 ppm comes from $LiNi_{0.5}Mn_{1.5}O_4$ in the positive electrode. It should be noted that the peak position of $LiNi_{0.5}Mn_{1.5}O_4$ in the *in situ* spectra is not equal to its isotropic shift (938 ppm as shown below). This is due to the bulk magnetic susceptibility effect, which causes additional peak shifts for metallic/paramagnetic

materials in the cell when the cell is flat-shaped and placed at non-magic angle with respect to the applied magnetic field.[50,51] We also note that the much larger signal intensity of $LiNi_{0.5}Mn_{1.5}O_4$ compared to the other Li components is a consequence of the pulse optimization for the former (for example, the pulse irradiation offset and relaxation delay).

Figures 1b and 1c show the drastic changes not only in intensity but also in peak position of $LiNi_{0.5}Mn_{1.5}O_4$ signal on charge-discharge process. We found the appearance of a new peak at ~1200 ppm, which can be attributed to the $Li_{0.5}$ phase as in the previous XRD studies.[7,18] The observed lower frequency shift is ascribable to the change in paramagnetic shift due to the valence change from Ni^{2+} (electron spin S = 1) to Ni^{3+} (S = 1/2) on the phase transformation from $Li_{1.0}$ to $Li_{0.5}$ phase.[16,18,20]

Figures 2a and 2b show the peak area ratio between the $Li_{1.0}$ and $Li_{0.5}$ phases along with charging profile. The peak area for each component was derived by the signal decomposition, which is shown in Supporting Information. We note that NMR spectroscopy is basically a quantitative analytical method, indicating that the changes in ^7Li signal intensity of the active material should be proportional to the charging or discharging capacities. However, it was found that the peak intensity of $LiNi_{0.5}Mn_{1.5}O_4$ immediately decreased at the onset of charging. The apparent intensity loss is larger than the consumed Li content estimated from the constant current density. This behavior corresponds to the build-up before voltage plateau at 4.73 V on the charging profile. Similar behavior has been also reported in the *in situ* NMR studies for $LiCoO_2$ and $Li_{1.08}Mn_{1.92}O_4$.[44,51] We suggested that the intensity loss can be ascribed to the signal decay before signal acquisition, since a severe electron-nuclear dipolar interaction induces a very rapid T_2 relaxation decay. The large intensity reduction at the very early delithiation stage is believed to be due to the

localized nature of the electron on paramagnetic ions and its nearby Li^+ ions.[25,44] Although $LiNi_{0.5}Mn_{1.5}O_4$ has only divalent Ni^{2+} and tetravalent Mn^{4+} ions in its theoretical composition, the active material used in this study showed a small deviation from the stoichiometry (see Experimental section), leading to the existence of a small amount of Mn^{3+} ion (< 3%). The $P4_332$ ordered spinel structure can accommodate a small deviation of the Ni/Mn ratio with the excess Mn atoms in 4*b* position.[8,10] $LiNi_xMn_{2-x}O_4$ ($0 < x < 0.5$) has a Mn^{3+}/Mn^{4+} redox couple at ~4 V, where delithiation proceeds in a solid solution reaction.[52] Therefore, we believe that the apparent intensity loss in NMR spectra at the onset of charging comes from a solid solution reaction associated with the Mn^{3+}/Mn^{4+} redox reaction below 4.7 V.

At the first plateau of 4.73 V, the ^7Li peak intensity of the $Li_{1.0}$ phase decreased monotonously, and that of the $Li_{0.5}$ phase increased in parallel (Figure 2b). The peak separation between the signals for $Li_{1.0}$ and $Li_{0.5}$ phases was barely enough to evaluate each signal intensity, and a pseudo-isosbestic point observed in the spectra for $0.55 \leq x \leq$ ~0.8 in $Li_xNi_{0.5}Mn_{1.5}O_4$ is a clear indication of the two-phase reaction between these phases (Figure S2b). The second plateau at 4.76 V corresponds to a monotonous intensity decrease of the $Li_{0.5}$ phase, originating from the second two-phase reaction between $Li_{0.5}$ and $Li_{0.0}$ phases, where the $Li_{0.0}$ phase has no Li content and therefore no contributions in the ^7Li NMR spectra.

On discharging process to 3.5 V, the intensity variations were reversible (Figures 2c and 2d). The cell was further discharged down to 2.0 V. Figure 1b shows a broader, asymmetric signal at the end of discharging, indicating that $LiNi_{0.5}Mn_{1.5}O_4$ can accommodate further lithium with different environments. The previous studies have reported that excess lithium

insertion into $LiNi_{0.5}Mn_{1.5}O_4$ leads to tetragonal $Li_2Ni_{0.5}Mn_{1.5}O_4$ ($Li_{2.0}$ phase).[11,13,15] A recent study pointed out that two voltage plateaus observed at ~2.7 V and ~2.1 V under non-equilibrium condition correspond to two tetragonal phases, stable T1 phase and metastable T2 phase, respectively.[11] The pseudo-isosbestic points observed in the *in situ* NMR spectra for $1.0 \leq x \leq 1.74$ in $Li_xNi_{0.5}Mn_{1.5}O_4$ indicates the two-phase reaction between $Li_{1.0}$ and $Li_{2.0}$ phases, but it seems difficult to discriminate the two peaks for the two $Li_{2.0}$ phases, T1 and T2 (Figure S2d). Moreover, the broad signals of $Li_{1.0}$ and $Li_{2.0}$ phases were heavily superposed each other, and it is difficult to decompose these two components without any assumptions. Here, we assumed that the last spectrum at 2.0 V ($Li_{1.74}Ni_{0.5}Mn_{1.5}O_4$ in bulk composition) was a mixture of $0.74Li_2Ni_{0.5}Mn_{1.5}O_4$ and $0.26LiNi_{0.5}Mn_{1.5}O_4$. Figures 2d shows the $Li_{1.0}$ phase decreasing in intensity along with the $Li_{2.0}$ phase increasing, confirming the two-phase reaction scheme between them. The sum of peak areas was largely deviated from the ideal line when excess lithium was inserted into $LiNi_{0.5}Mn_{1.5}O_4$. This is owing to the imperfect excitation of the broader signal of $Li_{2.0}$ phase, which shows multiple peaks with strong electron-nuclear dipolar interactions over wide frequency as mentioned below. We emphasize that our *in situ* ^{7}Li NMR measurement shows the changes in peak position as well as peak intensity on charge-discharge process, clearly suggesting the two-phase reactions between $Li_{1.0}$, $Li_{0.5}$, and $Li_{0.0}$ phases at the voltage window of 3.0 – 5.0 V, and between $Li_{1.0}$ and $Li_{2.0}$ phases at 2.0 – 3.0 V, respectively.

The *in situ* ^{7}Li NMR spectra of Li//$LiNi_{0.4}Mn_{1.6}O_4$ cell were shown in Figure 3 along with the corresponding electrochemical profile (Figure 3a). $LiNi_{0.4}Mn_{1.6}O_4$ showed a much broader signal centered at ~1400 ppm (the lowermost spectrum in Figure 3b). This broad

signal seems to move slightly to higher frequency before reaching to the ~4.7 V plateau, and then to lower frequency on further delithiation (Figure S6a). The slight positive shift below ~4.7 V can be attributed to the valence change of Mn^{3+} (S = 2) to Mn^{4+} (S = 3/2) in $LiNi_{0.4}Mn_{1.6}O_4$. Similar behavior has been reported for $Li_{1.08}Mn_{1.92}O_4$.[51] After the Mn^{3+}/Mn^{4+} redox reaction finished, the subsequent Ni^{2+}/Ni^{3+} redox reaction started and the signal moved to lower frequency.

The intensity variations in $Li_xNi_{0.4}Mn_{1.6}O_4$ along with the charging and discharging profiles were shown in Figure 4. In this case, the $Li_xNi_{0.4}Mn_{1.6}O_4$ signal was fitted with a single bi-gaussian function with the peak position and width being adjustable parameters. The good fitting with a single function is consistent with the observed continuous phase transition between $Li_{1.0}$ and $Li_{0.5}$ (Figure S18). Again, the peak intensity immediately decreased at the onset of charging (Figures 4a and 4b). The apparent intensity loss is larger than that observed in the ordered spinel $Li_xNi_{0.5}Mn_{1.5}O_4$, which may result from larger Mn^{3+} content in the disordered spinel $LiNi_{0.4}Mn_{1.6}O_4$. Below $x \approx 0.9$, the intensity monotonously decreased, although small intensity maximum was seen at $x \approx 0.5$ (Figure 3c). This apparent maximum seems to come from the signal narrowing at $x \approx 0.5$ (Figure S6b), which may be an indication of the completion of the continuous valence change from Ni^{2+} to Ni^{3+}, *i.e.*, $Li_{0.5}Ni_{0.4}Mn_{1.6}O_4$. On the discharging process, the intensity variations were reversible at the voltage window of 3.5 – 5.0 V (Figures 4c and 4d). Although the two-phase reaction between the $Li_{1.0}$ and $Li_{2.0}$ phases has been reported below 3.0 V,[11,13] it is very difficult to follow the reaction in the present spectra as they are overlapped with each other. Therefore, we only plotted the total intensity, which was again largely underestimated from the ideal line when excess lithium was inserted into $LiNi_{0.4}Mn_{1.6}O_4$. The reason of the deviation is

attributable to the imperfect excitation of the broader signal of $Li_{2.0}$ phase.

3-2. Detailed characterization of Li environments in ordered and disordered spinel

To examine the detailed local environment around Li ions, $LiNi_{0.5}Mn_{1.5}O_4$ and $LiNi_{0.4}Mn_{1.6}O_4$ electrode samples were also prepared by disassembling the cells at various charging and discharging states. Both the $P4_332$ and *Fd*-3*m* samples were characterized by XRD and Raman spectroscopy, which confirmed the occurrence of $Li_{1.0}$, $Li_{0.5}$, $Li_{0.0}$, and $Li_{2.0}$ phases (See Supporting Information). Figure 5 shows the spectral evolutions of ^6Li MAS NMR spectra for $LiNi_{0.5}Mn_{1.5}O_4$ electrodes, which were consistent with the above *in situ* NMR result, but more detailed structural information was provided. The spectrum of the soaked sample shows a sharp main signal at 938 ppm and a minor shoulder signal at 870 ppm (Figure 5a). The relative intensities of the 938 and 870 ppm signals including spinning sidebands were estimated to 96 and 4%, respectively. These signals belong to the $Li_{1.0}$ phase. According to the previous studies, they can be assigned to the Li ions in a crystallographic regular environment for $P4_332$ structure surrounded by $3Ni^{2+}/9Mn^{4+}$ ions, and in an irregular environment where the Li ion is surrounded by $2Ni^{2+}/10Mn^{3+,4+}$ ions or $3Ni^{2+}/9Mn^{3+,4+}$, respectively.[10,28,52,53] The latter environment was observed due to incomplete Ni/Mn ordering in the ordered spinel structure and/or small deviation from Ni/Mn stoichiometry related to the formation of trivalent Mn^{3+} ion. It is noted that the spectrum we obtained is similar in shape to that of $LiNi_{0.45}Mn_{1.55}O_4$ reported by Duncan *et al*, supporting a small Ni deficiency in our sample.[52] The presence of the minor signal suggests that the $P4_332$ ordered spinel can accommodate a small amount of Ni/Mn disordering, which may be dispersed in the structure as nano-scale domains.[12,53] On the

other hand, we believe that another minor signal at 710 ppm come from the impurity phase such as $Li_xNi_{1-x}O$[7,14] or $LiNiO_2$[28] (16 % of total Li), because this signal shows a strong dipolar interaction different from the others, and still exists in the spectrum of the 258 mAh/g-discharged sample (this signal is overlapped with the other peaks at 40 kHz MAS in Figure 5b; see also Figure S21d).[28] Charging to 15 mAh/g produced a small shift of the main signal to lower frequency (925 ppm), and a disappearance of the 870 ppm signal (Figure 5a). These features strongly suggest that Li ion was first deintercalated from the minor environment at 870 ppm where Mn^{3+} converted to Mn^{4+} during the initial raising the potential to 4.73 V, which corresponds to 15 mAh/g charging. The 710 ppm signal also decreased in intensity, suggesting the partial delithiation from the impurity phase. The 62 mAh/g-charged sample showed the $Li_{1.0}$ signal at ~920 ppm and a new sharp signal at 680 ppm. The latter can be explicitly attributed to the Li ions in the $Li_{0.5}$ phase. The phase transformation from $Li_{1.0}$ to $Li_{0.5}$ involves a valence change from Ni^{2+} to Ni^{3+}, leading to a new peak at lower frequency as shown in the above *in situ* NMR spectra. The existence of two separate signals from the $Li_{1.0}$ and $Li_{0.5}$ phases confirms a two-phase reaction. The $Li_{0.5}/Li_{1.0}$ phase ratio estimated from the ^6Li signal intensity was in excellent agreement with that from the Rietveld analyses (0.8/0.2 in phase ratio). The remnant Li signal from the $Li_{0.5}$ phase and a very small signal at ~525 ppm were observed in the spectrum of the 125 mAh/g-charged sample. Although the $Li_{0.0}$ phase is considered as Li-free phase in an ideal composition, we tentatively ascribed the latter signal to the Li environment residing in the $Li_{0.0}$ phase because the valence change from Ni^{3+} (S = 1/2) to Ni^{4+} (S = 0) would lead to an additional peak shift to much lower frequency. Then, the actual Li content in the $Li_{0.0}$ phase was estimated to be ~0.01Li, *i.e.*, $Li_{\sim 0.01}Ni_{0.5}Mn_{1.5}O_4$ in chemical composition, on the basis

of the relative intensity of the 525 and 680 ppm signals and the phase ratio obtained from the Rietveld analyses.

The spectrum of the 135 mAh/g-discharged sample was almost identical to that of soaked sample, indicating the reversible lithium extraction-insertion reaction (Figure 5b). The minor signal at 952 ppm was also recovered. It should be noted that the main and minor peaks shift toward higher frequencies than those observed in the soaked one. This is because of the difference in actual sample temperature coming from frictional heating on rotating at 40 or 60 kHz, the latter gives higher sample temperature, leading to a peak shift to lower frequency (40 kHz MAS was selected to avoid peak overlapping). On further discharging to 200 mAh/g, new signals were observed as well as the $Li_{1.0}$ signal. These new signals became prominent at 258 mAh/g discharging. We observed three isotropic shifts at 209, 307, and 943 ppm, all of which showed asymmetric spinning sideband manifolds, indicating their strong anisotropic electron-nuclear dipolar interactions. These signals should be assigned to the Li environments in the $Li_{2.0}$ phase, most probably in the T1 phase because the electrode sample was disassembled after long relaxation time reaching to ~2.7 V at open-circuit voltage.[11] A previous study has reported that the ^{6}Li MAS NMR spectra of lithium manganese oxides shift from 700 – 850 ppm for Mn^{4+}, to ~500 ppm for $Mn^{3.5+}$ (mixed valence), and to 36 – 143 ppm for Mn^{3+}-containing compounds.[24,26,28] Therefore, we tentatively consider that the two peaks at 209 and 307 ppm for $Li_{2.0}$ phase come from the Li environments close to Ni^{2+}/Mn^{3+} ions, and that at 943 ppm from the environments close to Ni^{2+}/Mn^{4+} in $Li_2Ni_{0.5}Mn_{1.5}O_4$, where 2/3Mn ions are trivalent and the other 1/3Mn ions are still tetravalent. Unfortunately, the crystal structure of this tetragonal phase has not yet been determined.[15] The determination of the crystal structure requires a high quality diffraction

profile of the target phase, but it is beyond the scope of this study. Hence, we discuss its possible structure based on our NMR results. By an analogy to $LiMn_2O_4$ (*Fd*-3*m*), the Ni/Mn-disordered $LiNi_{0.5}Mn_{1.5}O_4$ (*Fd*-3*m*) is considered to transform into the Ni/Mn-disordered $Li_2Ni_{0.5}Mn_{1.5}O_4$ ($I4_1/amd$) on lithium insertion. The Ni/Mn-ordered structure ($P4_332$) has a lower symmetry than *Fd*-3*m*, suggesting that the space group of its counterpart tetragonal phase is also different (lower) in symmetry from $I4_1/amd$ (e.g., $P4_32_12$, the subgroup of $P4_332$) and it would have three crystallographically distinct Li sites.

Figure 6 shows the ^{6}Li MAS NMR spectra for $LiNi_{0.4}Mn_{1.6}O_4$ electrodes disassembled at various charging and discharging states. The spectrum of the soaked sample for $LiNi_{0.4}Mn_{1.6}O_4$ shows a broad feature (Figure 6a), which was very different from that for $LiNi_{0.5}Mn_{1.5}O_4$. Such a difference can be attributed to the difference in Li local environment in between $P4_332$- and *Fd*-3*m*-structured spinel phases, as well as the small difference in chemical composition (although the *Fd*-3*m*-structured $LiNi_{0.5}Mn_{1.5}O_4$ prepared at 800 °C for 30 min showed a similar spectrum to that of $LiNi_{0.4}Mn_{1.6}O_4$), indicating that ^{6}Li NMR spectroscopy is sensitive to the Ni/Mn ordering around Li ions.[10,52] The spectrum is similar in shape to that of $LiNi_{0.35}Mn_{1.65}O_4$ (*Fd*-3*m*) reported by Duncan *et al.*, suggesting that the Li ions experience several environments arising from different $Ni/Mn^{3+,4+}$ arrangements.[52] The peak maximum at ~820 ppm indicates the predominance of $2Ni^{2+}/10Mn^{4+,3+}$ and $1Ni^{2+}/11Mn^{4+,3+}$ arrangements in $LiNi_{0.4}Mn_{1.6}O_4$.[10] Additional signal at 700 ppm comes from the impurity phase, whose intensity was increased from 16% to 28% of total Li by the calcination at 900 °C for 6 h. The 15 mAh/g-charged sample showed a small positive shift of the spinel signal to 850 ppm, corresponding to the valence change of

some Mn^{3+} to Mn^{4+}.[24,27] Charging to 60 mAh/g lead to a peak shift to lower frequency. This signal can be attributed to the Li ions in the $Li_{0.5}$ phase according to the supporting XRD measurements (Figures S17 and S18). These XRD results suggest that the phase transformation from $Li_{1.0}$ to $Li_{0.5}$ is a single-phase reaction in the *Fd*-3*m* spinel, where the valence change occurs in the randomly 16*c*-occupying Ni ions from divalent to trivalent and the cell volume decreases continuously.[7,9,52] We note that the oxidation of Ni ion provides a negative frequency shift, while that of Mn ion provides a positive shift. In the 115 mAh/g-charged sample, the peak position further shifted down to ~700 ppm. We believe that this signal comes from the remaining $Li_{0.5}$ phase, although some contributions from the impurity phase, as observed in the soaked and 15 mAh/g-charged samples, may be included.

On the discharging process, the 115 mAh/g-discharged sample showed a spectrum similar to that of soaked one (Figure 6b). The spectrum of the 228 mAh/g-discharged sample shows a new broad signal at ~470 ppm, which can be attributed to the Li environments in the $Li_{2.0}$ phase. We note that the spectrum is very different from that of the $Li_{2.0}$ phase coming from $P4_332$ structure as shown above (See also Figure S21d). If we believe that the $Li_{2.0}$ phase coming from *Fd*-3*m* structure adopts the space group $I4_1/amd$, the broad signal at ~470 ppm would be attributed to the 8*c* octahedral site in Wyckoff position, which was proposed for Li occupation in $Li_2Mn_2O_4$,[54] although an earlier study had suggested both the 4*a* tetrahedral and 8*c* octahedral sites.[55] The broad feature reflects the random occupation of Ni/Mn ions in 8*d* site.

4. Conclusions

We carried out an intensive characterization of ordered spinel $LiNi_{0.5}Mn_{1.5}O_4$ and disordered spinel $LiNi_{0.4}Mn_{1.6}O_4$ on charge-discharge process by using *in situ* (*in operando*) ^{7}Li NMR and ^{6}Li MAS NMR spectroscopy. The present study provided the fundamental information on how the Li environments in the active materials change during electrochemical delitiation and lithiation reaction as well as the crystal or electronic structures do. The *in situ* ^{7}Li monitoring of the ordered spinel on delithiation revealed the appearance and subsequent disappearance of a new signal from $Li_{0.5}Ni_{0.5}Mn_{1.5}O_4$, indicating the two-phase reaction processes among $Li_{1.0}Ni_{0.5}Mn_{1.5}O_4$, $Li_{0.5}Ni_{0.5}Mn_{1.5}O_4$, and $Li_{0.0}Ni_{0.5}Mn_{1.5}O_4$. In contrast, the disordered spinel did not show clear two-phase reaction process between $Li_{1.0}Ni_{0.4}Mn_{1.6}O_4$ and $Li_{0.5}Ni_{0.4}Mn_{1.6}O_4$, which is consistent with a continuous phase transition between them. The ^{7}Li intensity variations revealed that both the ordered and disordered spinel phases had a single-phase reaction process at the onset of charging, which resulted from Mn^{3+}/Mn^{4+} redox reaction. Also, the *in situ* monitoring suggested that the Ni/Mn ordering in $P4_332$ and disordering in *Fd*-3*m* were kept during charge-discharge process. ^{6}Li MAS NMR spectra of the electrode samples disassembled at various Li contents also supported the *in situ* result. The present results are in contrast with the previous study showing no significant evolution in peak position during delithiation.[28] We believe that their samples were subjected to moisture or oxygen before NMR measurements, which would decompose the unstable $Li_{0.5}$ phase (into, for example, Li_2CO_3 and Li-free transition-metal oxides) but the $Li_{1.0}$ phase was stable and alive. The application of *in situ* and *ex situ* NMR techniques has confirmed that the evolutions of Li local environments in the ordered and disordered spinel phases on charge-discharge process are different from each other and are consistent with those of their crystal and electronic

structures. This underlines that the Li environments are strongly affected by the framework structures (bond angles, interatomic distances, and lattice parameters) and especially by the electronic structures (valence states) of the surrounding transition-metal ions.

Acknowledgments

This work was supported by the Research and Development Innovative for Scientific Innovation of New Generation Battery (RISING) project from New Energy and Industrial Technology Development Organization (NEDO), Japan. The authors thank Mr. Takahiro Kakei for his supports on electrochemical sample preparations, and Mr. Takashi Moroishi for his supports on NMR measurements.

Supporting Information Available: The details of the fitting procedure of the *in situ* NMR spectra, and characterizations of the electrode samples by XRD and Raman spectroscopy are summarized in the Supporting Information. This information is available free of charge via the Internet at http://pubs.acs.org.

References

(1) Tarascon, J. M.; Armand, M. Issues and Challenges Facing Rechargeable Lithium Batteries. *Nature* **2001**, *414*, 359–367.

(2) Armand, M.; Tarascon, J. M. Building Better Batteries. *Nature* **2008**, *451*, 652–657.

(3) Wagner, F. T.; Lakshmanan, B.; Mathias, M. F. Electrochemistry and Future of the Automobile. *J. Phys. Chem. Lett.* **2010**, *1*, 2204–2219.

(4) Manthiram, A.; Chemelewski, K.; Lee, E.-S. A Perspective on the High-Voltage $LiMn_{1.5}Ni_{0.5}O_4$ Spinel Cathode for Lithium-Ion Batteries. *Energy Environ. Sci.* **2014**, *7*, 1339–1350.

(5) Kim, J.-H.; Pieczonka, N. P. W.; Yang, L. Challenges and Approaches for High-Voltage Spinel Lithium-Ion Batteries. *ChemPhysChem* **2014**, *15*, 1940–1954.

(6) Kim, J.-H.; Myung, S.-T.; Yoon, C. S.; Kang, S. G.; Sun, Y.-K. Comparative Study of $LiNi_{0.5}Mn_{1.5}O_{4-\delta}$ and $LiNi_{0.5}Mn_{1.5}O_4$ Cathodes Having Two Crystallographic Structures: *Fd*3*m* and $P4_332$. *Chem. Mater.* **2004**, *16*, 906–914.

(7) Kunduraci, M; Amatucci, G. G. Synthesis and Characterization of Nanostructured 4.7 V $Li_xNi_{0.5}Mn_{1.5}O_4$ Spinels for High-Power Lithium-Ion Batteries. *J. Electrochem. Soc.* **2006**, *153*, A1345–1352.

(8) Pasero, D.; Reeves, N.; Pralong, V.; West, A. R. Oxygen Nonstoichiometry and Phase Transitions in $LiNi_{0.5}Mn_{1.5}O_{4-\delta}$. *J. Elctrochem. Soc.* **2008**, *155*, A282–291.

(9) Wang, L.; Li, H.; Huang, X.; Baudrin, E. A Comparative Study of Fd-3m and $P4_332$ "$LiNi_{0.5}Mn_{1.5}O_4$". *Solid State Ionics* **2011**, *193*, 32–38.

(10) Cabana, J.; Casas-Cabanas, M.; Omenya, F. O.; Chernova, N. A.; Zeng, D.; Whittingham, M. S.; Grey, C. P. Composition-Structure Relationships in the Li-Ion

Battery Electrode Material $LiNi_{0.5}Mn_{1.5}O_4$. *Chem. Mater.* **2012**, *24*, 2952–2964.

(11) Lee, E.-S.; Nam, K.-W.; Hu, E.; Manthiram, A. Influence of Cation Ordering and Lattice Distortion on the Charge-Discharge Behavior of $LiNi_{0.5}Mn_{1.5}O_4$ Spinel between 5.0 and 2.0 V. *Chem. Mater.* **2012**, *24*, 3610–3620.

(12) Kim, J.-H.; Huq, A.; Chi, M.; Pieczonka, N. P. W.; Lee, E.; Bridges, C. A.; Tessema, M. M. ; Manthiram, A.; Persson, K. A.; Powell, B. R. Integrated Nano-Domains of Disordered and Ordered Spinel Phases in $LiNi_{0.5}Mn_{1.5}O_4$ for Li-Ion Batteries. *Chem. Mater.* **2014**, *26*, 4377–4386.

(13) Park, S. H.; Oh, S.-W.; Kang, S. H.; Belharouak, I.; Amine, K.; Sun, Y.-K. Comparative Study of Different Crystallographic Structure of $LiNi_{0.5}Mn_{1.5}O_{4-\delta}$ Cathodes with Wide Operation Voltage (2.0–5.0 V). *Electrochim. Acta* **2007**, *52*, 7226–7230.

(14) Zhong, Q.; Bonakdarpour, A.; Zhang, M.; Gao, Y.; Dahn, J. R. Synthesis and Electrochemistry of $LiNi_xMn_{2-x}O_4$. *J. Electrochem. Soc.* **1997**, *144*, 205–213.

(15) Ariyoshi, K.; Iwakoshi, Y.; Nakayama, N.; Ohzuku, T. Topotactic Two-Phase Reactions of $Li[Ni_{1/2}Mn_{3/2}]O_4$ ($P4_332$) in Nonaqueous Lithium Cells. *J. Electrochem. Soc.* **2004**, *151*, A296–303.

(16) Hayakawa, N.; Kawai, T.; Sakai, H.; Honda, A.; Oyama, T.; Yamanaka, K.; Yogi, C.; Ohta, T. Chemical State Analysis of $Li_{1-x}Ni_{0.5}Mn_{1.5}O_4$ by Soft X-ray Absorption Specroscopy. *Hyomenkagaku* **2013**, *34*, 415–420 (in Japanese).

(17) Okumura, T.; Shikano, M.; Kobayashi, H. Contribution of Oxygen Partial Density of State on Lithium Intercalation/De-Intercalation Process in $Li_xNi_{0.5}Mn_{1.5}O_4$ Spinel Oxides. *J. Power Sources* **2013**, *244*, 544–547.

(18) Arai, H.; Sato, K.; Orikasa, Y.; Murayama, H.; Takahashi, I.; Koyama, Y.; Uchimoto, Y.; Ogumi, Z. Phase Transition Kinetics of $LiNi_{0.5}Mn_{1.5}O_4$ Electrodes Studied by *In Situ* X-ray Absorption Near-Edge Structure and X-ray Diffraction Analysis. *J. Mater. Chem. A* **2013**, *1*, 10442–10449.

(19) Rana, J.; Glatthaar, S.; Gesswein, H.; Sharma, N.; Binder, J. R.; Chernikov, R.; Schumacher, G.; Banhart, J. Local Structural Changes in $LiNi_{0.5}Mn_{1.5}O_4$ Spinel Cathode Material for Lithium-Ion Batteries. *J. Power Sources* **2014**, *255*, 439–449.

(20) Zhou, J.; Hong, D.; Wang, J.; Hu, Y.; Xie, X.; Fang, H. Electronic Structure Variation of the Surface and Bulk of a $LiNi_{0.5}Mn_{1.5}O_4$ Cathode as a Function of State of Charge: X-ray Absorption Spectroscopic Study. *Phys. Chem. Chem. Phys.* **2014**, *16*, 13838–13842.

(21) Morgan, K. R.; Collier, S.; Burns, G.; Ooi, K. A ^{6}Li and ^{7}Li MAS NMR Study of the Spinel-Type Manganese Oxide $LiMn_2O_4$ and the Rock Salt-Type Manganese Oxide Li_2MnO_3. *J. Chem. Soc. Chem. Commun.* **1994**, 1719–1720.

(22) Marichal, C.; Hirschinger, J.; Granger, P.; Ménétrier, M.; Rougier, A.; Delmas, C. ^{6}Li and ^{7}Li NMR in the $LiNi_{1-y}Co_yO_2$ Solid Solution ($0 \leq y \leq 1$). *Inorg. Chem.* **1995**, *34*, 1773–1778.

(23) Mustarelli, P.; Massarotti, V.; Bini, M.; Capsoni, D. Transferred Hyperfine Interaction and Structure in $LiMn_2O_4$ and Li_2MnO_3 Coexisting Phases: A XRD and ^{7}Li NMR-MAS Study. *Phys. Rev. B* **1997**, *55*, 12018–12024.

(24) Lee, Y. J.; Wang, F.; Grey, C. P. ^{6}Li and ^{7}Li MAS NMR Studies of Lithium Manganate Cathode Materials. *J. Am. Chem. Soc.* **1998**, *120*, 12601–12613.

(25) Ménétrier, M.; Saadoune, I.; Levasseur, S.; Delmas, C. The Insulator-Metal

Transition upon Lithium Deintercalation from $LiCoO_2$: Electronic Properties and ^7Li NMR Study. *J. Mater. Chem.* **1999**, *9*, 1135–1140.

(26) Lee, Y. J.; Grey, C. P. ^6Li Magic-Angle Spinning (MAS) NMR Study of Electron Correlations, Magnetic Ordering, and Stability of Lithium Manganese(III) Oxides. *Chem. Mater.* **2000**, *12*, 3871–3878.

(27) Lee, Y. J.; Wang, F.; Mukerjee, S.; McBreen, J.; Grey, C. P. ^6Li and ^7Li Magic-Angle Spinning Nuclear Magnetic Resonance and *In Situ* X-ray Diffraction Studies of the Charging and Discharging of $Li_xMn_2O_4$ at 4 V. *J. Electrochem. Soc.* **2000**, *147*, 803–812.

(28) Lee, Y. J.; Eng, C.; Grey, C. P. ^6Li Magic Angle Spinning NMR Study of the Cathode Material $LiNi_xMn_{2-x}O_4$. *J. Electrochem. Soc.* **2001**, *148*, A249–257.

(29) Lee, Y. J.; Park, S.-H.; Eng, C.; Parise, J. B.; Grey, C. P. Cation Ordering and Electrochemical Properties of the Cathode Materials $LiZn_xMn_{2-x}O_4$, $0 < x \leq 0.5$: A ^6Li Magic-Angle Spinning NMR Spectroscopy and Diffraction Study. *Chem. Mater.* **2002**, *14*, 194–205.

(30) Grey, C. P.; Dupré, N. NMR Studies of Cathode Materials for Lithium-Ion Rechargeable Batteries. *Chem. Rev.* **2004**, *104*, 4493–4512.

(31) Armstrong, A. R.; Dupré, N.; Paterson, A. J.; Grey, C. P.; Bruce, P. G. Combined Neutron Diffraction, NMR, and Electrochemical Investigation of the Layered-to-Spinel Transformation in $LiMnO_2$. *Chem. Mater.* **2004**, *16*, 3106–3118.

(32) Cahill, L. S.; Yin, S.-C.; Samoson, A.; Heinmaa, I.; Nazar, L. F.; Goward, G. R. ^6Li NMR Studies of Cation Disorder and Transition Metal Ordering in $Li[Ni_{1/3}Mn_{1/3}Co_{1/3}]O_2$ Using Ultrafast Magic Angle Spinning. *Chem. Mater.* **2005**, *17*,

6560–6566.

(33) Chazel, C.; Ménétrier, M.; Croguennec, L.; Delmas, C. Coupled Ion/Electron Hopping in Li_xNiO_2: A ^{7}Li NMR Study. *Inorg. Chem.* **2006**, *45*, 1184–1191.

(34) Cabana, J.; Kang, S.-H.; Johnson, C. S.; Thackeray, M. M.; Grey, C. P. Structural and Electrochemical Characterization of Composite Layered-Spinel Electrodes Containing Ni and Mn for Li-Ion Batteries. *J. Electrochem. Soc.* **2009**, *156*, A730–736.

(35) Sirisopanaporn, C.; Dominko, R.; Masquelier, C.; Armstrong, A. R.; Mali, G.; Bruce, P. G. Polymorphism in $Li_2(Fe,Mn)SiO_4$: A Combined Diffraction and NMR Study. *J. Mater. Chem.* **2011**, *21*, 17823–17831.

(36) Shimoda, K.; Sugaya, H.; Murakami, M.; Arai, H.; Uchimoto, Y.; Ogumi, Z. Characterization of Bulk and Surface Chemical States on Electrochemically Cycled $LiFePO_4$: A Solid State NMR Study. *J. Electrochem. Soc.* **2014**, *161*, A1012–1018.

(37) Murakami, M.; Noda, Y.; Koyama, Y.; Takegoshi, K.; Arai, H.; Uchimoto, Y.; Ogumi, Z. Local Structure and Spin State of Cobalt Ion at Defect in Lithium Overstoichiometric $LiCoO_2$ As Studied by $^{6/7}$Li Solid-State NMR Spectroscopy. *J. Phys. Chem. C* **2014**, *118*, 15375–15385.

(38) Gerald II, R. E.; Klingler, R. J.; Sandí, G.; Johnson, C. S.; Scanlon, L. G.; Rathke, J. W. ^{7}Li NMR Study of Intercalated Lithium in Curved Carbon Lattices. *J. Power Sources* **2000**, *89*, 237–243.

(39) Gerald II, R. E.; Sanchez, J.; Johnson, C. S.; Klingler, R. J.; Rathke, J. W. *In Situ* Nuclear Magnetic Resonance Investigations of Lithium Ions in Carbon Electrode Materials Using a Novel Detector. *J. Phys.: Condens. Matter* **2001**, *13*, 8269–8285.

(40) Letellier, M.; Chevallier, F.; Clinard, C.; Frackowiak, E.; Rouzaud, J.-N.; Béguin,

F. The First *In Situ* ^{7}Li Nuclear Magnetic Resonance Study of Lithium Insertion in Hard-Carbon Anode Materials for Li-Ion Batteries. *J. Chem. Phys.* **2003**, *118*, 6038–6045.

(41) Letellier, M.; Chevallier, F.; Morcrette, M. In Situ ^{7}Li Nuclear Magnetic Resonance Observation of the Electrochemical Intercalation of Lithium in Graphite; 1st Cycle. *Carbon* **2007**, *45*, 1025–1034.

(42) Key, B.; Bhattacharyya, R.; Morcrette, M.; Seznéc, V.; Tarascon, J.-M.; Grey, C. P. Real-Time NMR Investigations of Structural Changes in Silicon Electrodes for Lithium-Ion Batteries. *J. Am. Chem. Soc.* **2009**, *131*, 9239–9249.

(43) Chevallier, F.; Poli, F.; Montigny, B.; Letellier, M. *In Situ* ^{7}Li Nuclear Magnetic Resonance Observation of the Electrochemical Intercalation of Lithium in Graphite: Second Cycle Analysis. *Carbon* **2013**, *61*, 140–153.

(44) Shimoda, K.; Murakami, M.; Takamatsu, D.; Arai, H.; Uchimoto, Y.; Ogumi, Z. *In Situ* NMR Observation of the Lithium Extraction/Insertion from $LiCoO_2$ Cathode. *Electrochim. Acta* **2013**, *108*, 343–349.

(45) Ogata, K.; Salager, E.; Kerr, C. J.; Fraser, A. E.; Ducati, C.; Morris, A. J.; Hofmann, S.; Grey, C. P. Revealing Lithium-Silicide Phase Transformations in Nano-Structured Silicon-Based Lithium Ion Batteries via *In Situ* NMR Spectroscopy. *Nature Commun.* **2014**, *5*:3217.

(46) Gotoh, K.; Izuka, M.; Arai, J.; Okada, Y.; Sugiyama, T.; Takeda, K.; Ishida, H. *In Situ* ^{7}Li Nuclear Magnetic Resonance Study of the Relaxation Effect in Practical Lithium Ion Batteries. *Carbon* **2014**, *79*, 380–387.

(47) Salager, E.; Sarou-Kanian, V.; Sathiya, M.; Tang, M.; Leriche, J.-B.; Melin, P.;

Wang, Z.; Verin, H.; Bassada, C.; Deschamps, M. et al. Solid-State NMR of the Family of Positive Electrode Materials $Li_2Ru_{1-y}Sn_yO_3$ for Lithium-Ion Batteries. *Chem. Mater.* **2014**, *26*, 7009–7019.

(48) Jung, H.; Allan, P. K.; Hu, Y.-Y.; Borkiewicz, O. J.; Wang, X.-L.; Han, W.-Q.; Du, L.-S.; Pickard, C. J.; Chupas, P. J.; Chapman, K. W. et al. Elucidation of the Local and Long-Range Structural Changes that Occur in Germanium Anodes in Lithium-Ion Batteries. *Chem. Mater.* **2015**, *27*, 1031–1041.

(49) Bielecki, A.; Burum, D. Temperature Dependence of ^{207}Pb MAS Spectra of Solid Lead Nitrate. An Accurate, Sensitive Thermometer for Variable-Temperature MAS. *J. Magn. Reson. A* **1995**, *116*, 215–220.

(50) Trease, N. M.; Zhou, L.; Chang, H. J.; Zhu, B. Y.; Grey, C. P. *In Situ* NMR of Lithium Ion Batteries: Bulk Susceptibility Effects and Practical Considerations. *Solid State Nucl. Magn. Reson.* **2012**, *42*, 62–70.

(51) Zhou, L.; Leskes, M.; Ilott, A. J.; Trease, N. M.; Grey, C. P. Paramagnetic Electrodes and Bulk Magnetic Susceptibility Effects in the *In Situ* NMR Studies of Batteries: Application to $Li_{1.08}Mn_{1.92}O_4$ Spinels. *J. Magn. Reson.* **2013**, *234*, 44–57.

(52) Duncan, H.; Hai, B. Leskes, M.; Grey, C. P.; Chen, G. Relationships between Mn^{3+} Content, Structural Ordering, Phase Transformation, and Kinetic Properties in $LiNi_xMn_{2-x}O_4$ Cathode Materials. *Chem. Mater.* **2014**, *26*, 5374–5382.

(53) Ivanova, S.; Zhecheva, E.; Stoyanova, R.; Nihtianova, D.; Wegner, S.; Tzvetkova, P.; Simova, S. High-Voltage $LiNi_{1/2}Mn_{3/2}O_4$ Spinel: Cationic Order and Particle Size Distribution. *J. Phys. Chem. C* **2011**, *115*, 25170–25182.

(54) Wills, A. S.; Raju, N. P.; Morin, C.; Greedan, J. E. Two-Dimensional Short-Range

Magnetic Order in the Tetragonal Spinel $Li_2Mn_2O_4$. *Chem. Mater.* **1999**, *11*, 1936–1941.

(55) David, W. I. F.; Thackeray, M. M.; de Picciotto, L. A.; Goodenough, J. B. Structure Refinement of the Spinel-Related Phases $Li_2Mn_2O_4$ and $Li_{0.2}Mn_2O_4$. *J. Solid State Chem.* **1987**, *67*, 316–323.

Figures and Figure captions

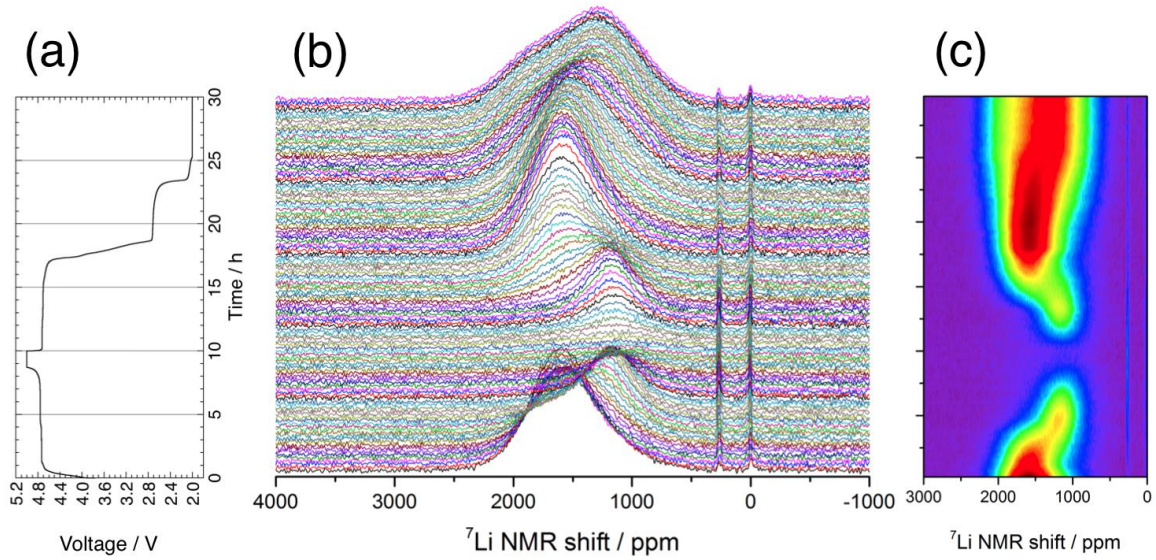

Figure 1. *In situ* ^{7}Li static NMR spectra of Li//$LiNi_{0.5}Mn_{1.5}O_4$ ($P4_332$ structure) cell. (a) Charge-discharge profile (0.1C rate) as a function of time, (b) stacked and (c) contour plots of *in situ* ^{7}Li spectra.

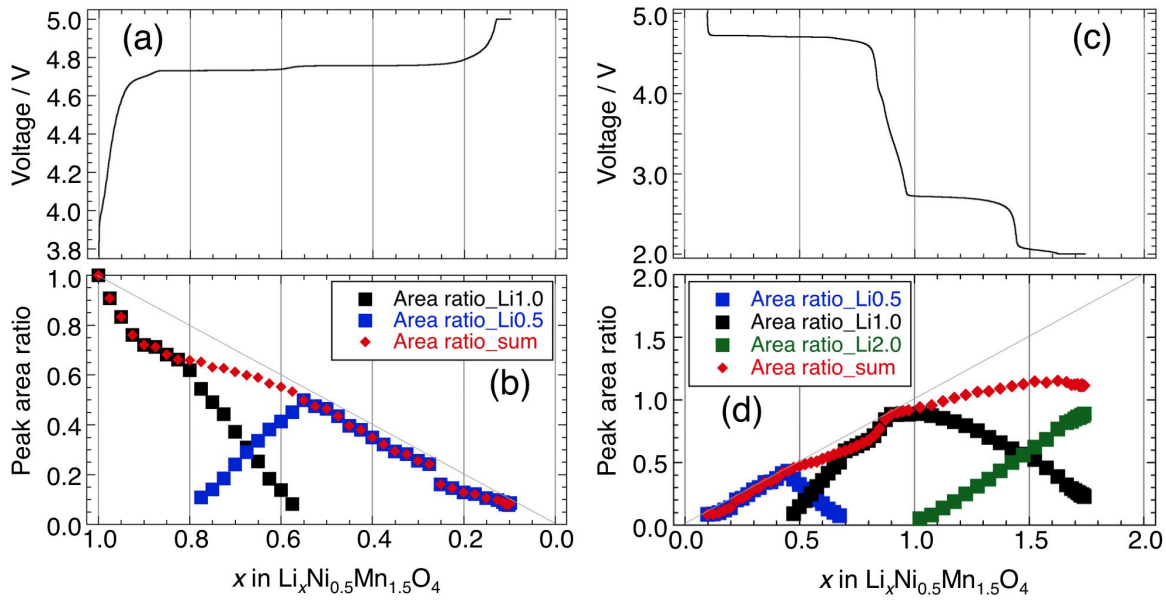

Figure 2. (a) Charging profile up to 5.0 V, and (b) peak area ratio of the $Li_{1.0}$ and $Li_{0.5}$ phase components decomposed from *in situ* ^{7}Li spectra of the $LiNi_{0.5}Mn_{1.5}O_4$ electrode. (c) Discharging profile down to 2.0 V, and (d) peak area ratio of the $Li_{0.5}$, $Li_{1.0}$, and $Li_{2.0}$ phase components.

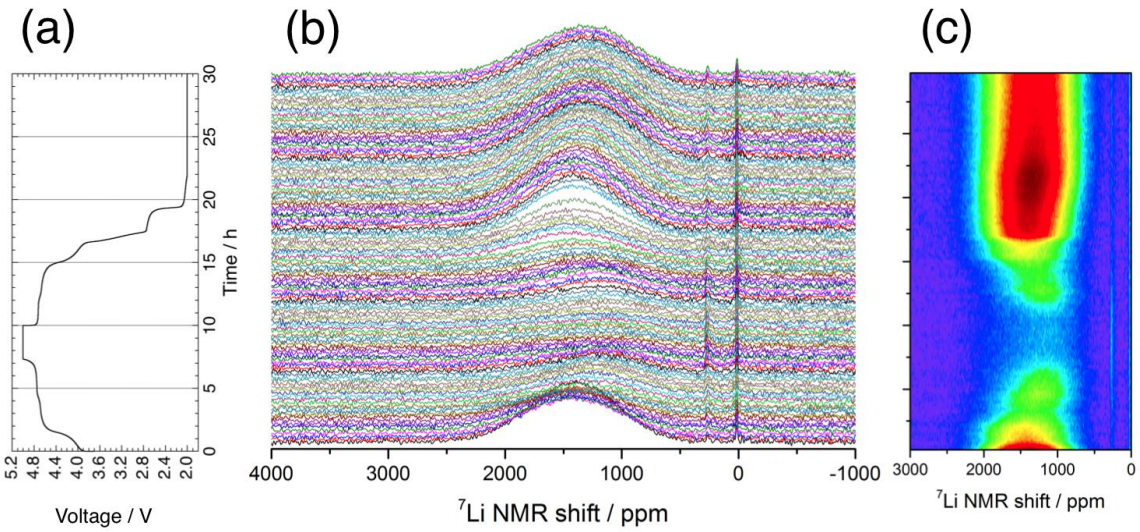

Figure 3. *In situ* ^{7}Li static NMR spectra of Li//$LiNi_{0.4}Mn_{1.6}O_4$ (*Fd*-3*m* structure) cell. (a) Charge-discharge profile (0.1C rate) as a function of time, (b) stacked and (c) contour plots of *in situ* ^{7}Li spectra.

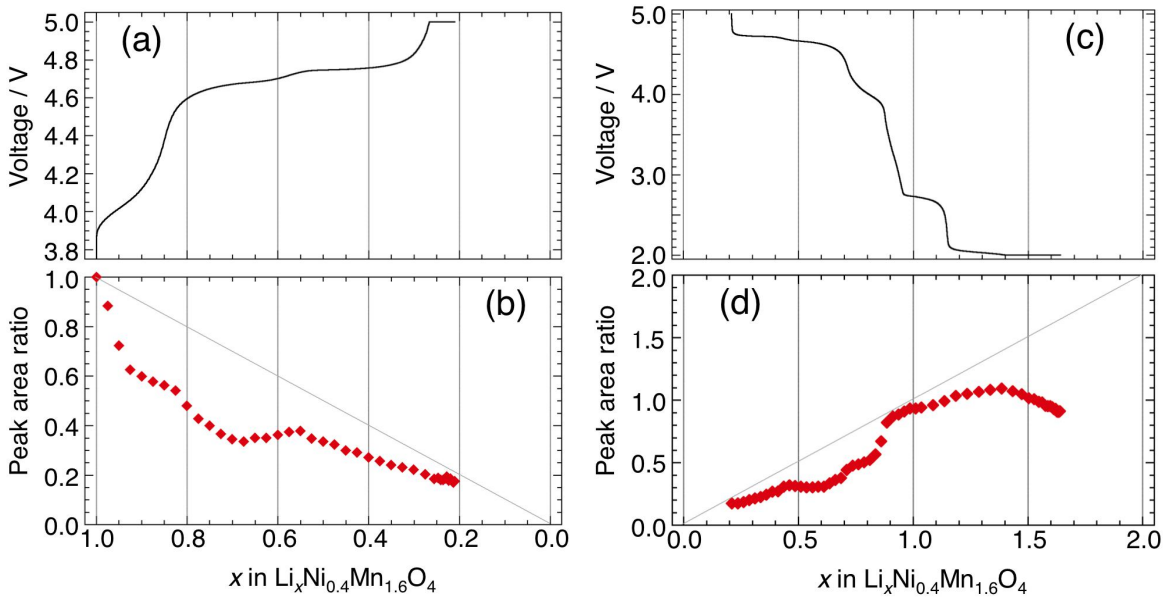

Figure 4. (a) Charging profile up to 5.0 V, and (b) peak area extracted from *in situ* ^{7}Li spectra of the $LiNi_{0.4}Mn_{1.6}O_4$ electrode. (c) Discharging profile down to 2.0 V, and (d) peak area variation.

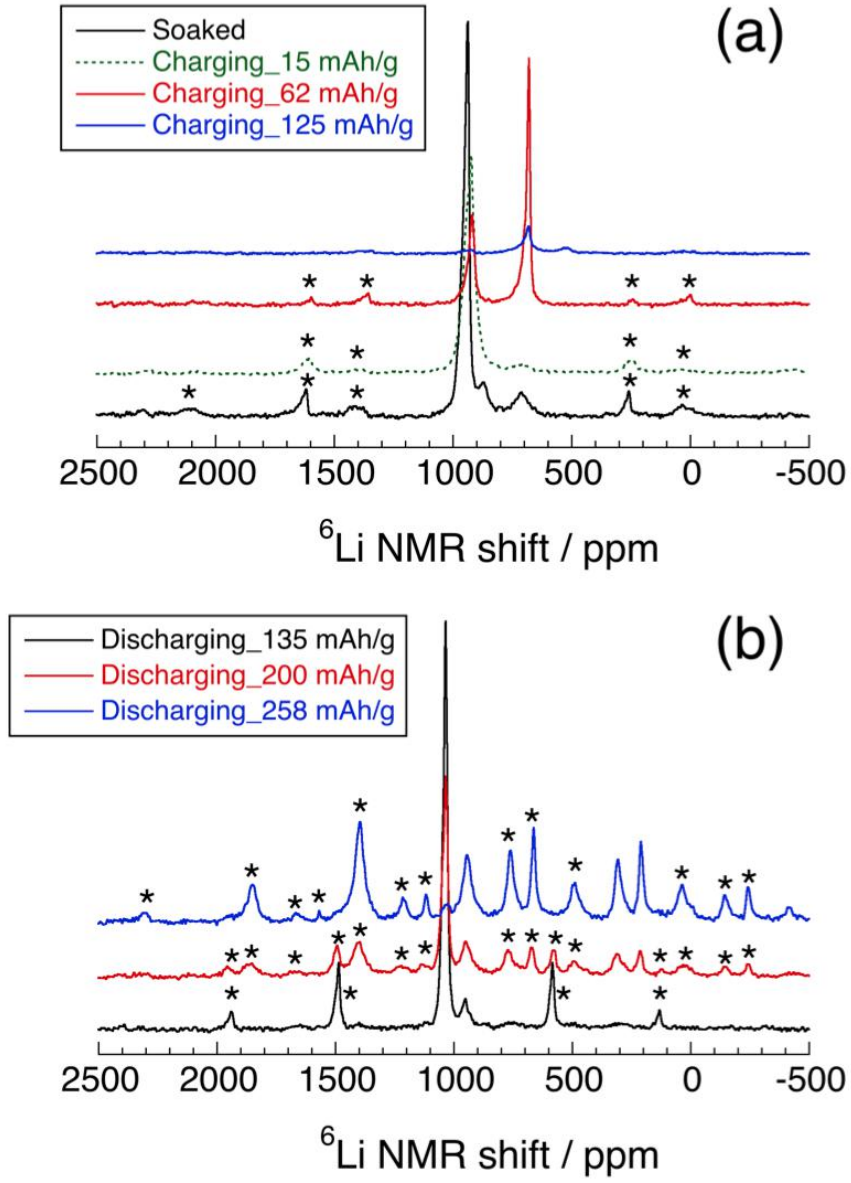

Figure 5. ^{6}Li MAS NMR spectra of the $LiNi_{0.5}Mn_{1.5}O_4$ electrode disassembled on (a) charging process to 5.0 V, and (b) discharging process to 2.0 V. These were acquired at a MAS rate of 60 kHz and 40 kHz, respectively. Asterisks indicate spinning sidebands. Spectra were normalized for sample weight and scan numbers, and stacked upward for clarity.

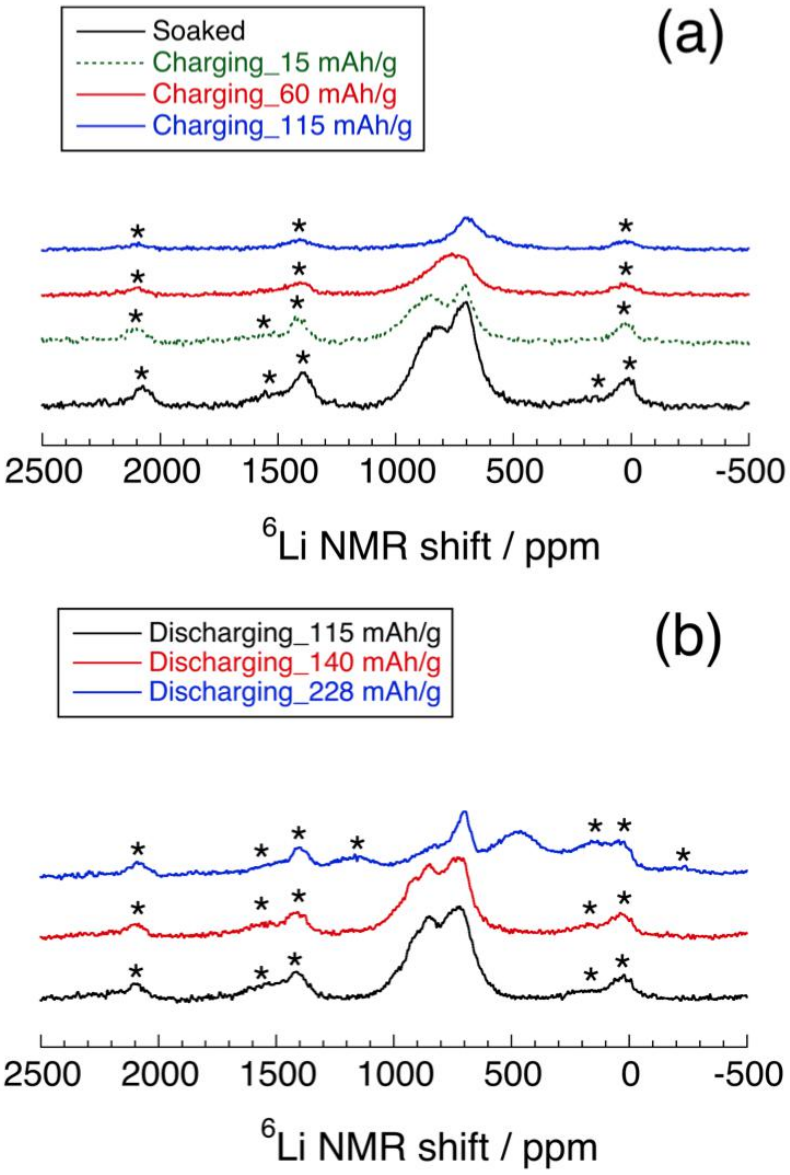

Figure 6. ^{6}Li MAS NMR spectra of the $LiNi_{0.4}Mn_{1.6}O_4$ electrode disassembled on (a) charging process to 5.0 V, and (b) discharging process to 2.0 V. These were all acquired at a MAS rate of 60 kHz. Asterisks indicate spinning sidebands. Spectra were normalized for sample weight and scan numbers, and stacked upward for clarity.

Table of Content